ACS APPLIED MATERIALS & INTERFACES

Research Article

www.acsami.org

Adsorption of Lipid Liquid Crystalline Nanoparticles on Cationic, Hydrophilic, and Hydrophobic Surfaces

Debby P. Chang,*[,†] Marija Jankunec,[‡] Justas Barauskas,[‡,§] Fredrik Tiberg,[†,∥] and Tommy Nylander[†]

[†]Department of Physical Chemistry, Lund University, P.O. Box 124, SE-22100 Lund, Sweden

[‡]Vilnius University Institute of Biochemistry, Mokslininkų 12, LT-08662 Vilnius, Lithuania

[§]Department of Biomedical Science, Faculty of Health and Society, Malmö University, SE-20506 Malmö, Sweden

[∥]Camurus AB, Ideon Science Park, SE-22370 Lund, Sweden

Supporting Information

ABSTRACT: Investigation of nonlamellar nanoparticles formed by dispersion of self-assembled lipid liquid crystalline phases is stimulated by their many potential applications in science and technology; resulting from their unique solubilizing, encapsulating, and space-dividing nature. Understanding the interfacial behavior of lipid liquid crystalline nanoparticles (LCNPs) at surfaces can facilitate the exploitation of such systems for a number of potentially interesting uses, including preparation of functional surface coatings and uses as carriers of biologically active substances. We have studied the adsorption of LCNP, based on phosphatidylcholine/glycerol dioleate and Polysorbate 80 as stabilizers, at different model surfaces by use of in situ ellipsometry. The technique allows time-resolved monitoring of the layer thickness and the amount adsorbed, thereby providing insights into the restructuring of the lipid nanoparticle upon adsorption. The effects of solvent condition, electrolyte concentration, particle size, and surface chemistry on adsorbed layer properties were investigated. Furthermore, the internal structures of the particles were investigated by cryo-transmission electron microscopy and small angle X-ray diffraction on the corresponding liquid crystalline phases in excess water. LCNPs are shown to form well-defined layers at the solid−liquid interface with a structure and coverage that are determined by the interplay between the self-assembly properties of the lipids and lipid surface interactions, respectively. At the hydrophobic surface, hydrophobic interaction results in a structural transition from the original LCNP morphology to a monolayer structure at the interface. In contrast, at cationic and hydrophilic surfaces, relaxation is a relatively slow process, resulting in much thicker adsorbed layers, with thickness and adsorption behavior that to a greater extent reflect the original bulk LCNP properties.

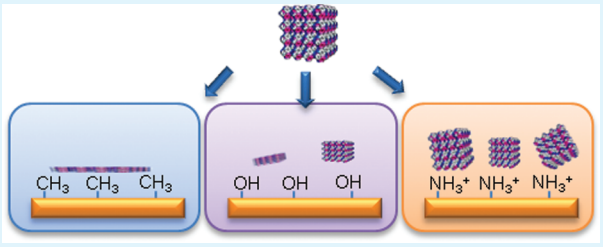

KEYWORDS: *lipid liquid crystalline nanoparticle, cubosome, adsorption, ellipsometry, cationic, SPC, GDO, P80, cryo-TEM, nanoparticles*

INTRODUCTION

Reversed nonlamellar lipid-based liquid crystalline structures, such as cubic, hexagonal, and sponge phases, have potential applications as carriers and delivery systems in pharmaceutical, food, and cosmetic applications. This is due to the space-dividing nature of these phases that features mono- or bicontinuous networks of both hydrophilic and hydrophobic domains, allowing the incorporation of different substances ranging from hydrophobic or hydrophilic molecules to amphiphilic peptides.[1,2] In many applications, it is an advantage to disperse liquid crystalline phases into particles in excess water using an appropriate fragmentation and dispersion stabilizer, as this reduces viscosity and facilitates administration and delivery. Such particle-based systems can be produced with excellent long-term colloidal stability and retained internal phase morphology.[3,4]

One of the most widely studied lipid liquid crystalline nanoparticles (LCNPs) is the bicontinuous cubic-phase nanoparticle, termed the cubosome, from glycerol monooleate (GMO). GMO is commercially available as a food emulsifier.[5] The lipid forms a reversed bicontinuous cubic phase in excess water, which can be dispersed into colloidal nanoparticles in aqueous solution using high shear and an amphiphilic stabilizer, for example, a triblock copolymer.[3,6,7] The system has been extensively studied with regard to physicochemical properties and as carrier system for a wide variety of drug substances.[1] Although a promising candidate for several applications, GMO-based LCNPs have been shown to exhibit some hemolytic activity at higher concentrations,[8] reducing their potential as carriers for use in intravenous drug delivery.

A recent study demonstrated that exchanging the GMO lipid for a mixture of soy phosphatidylcholine (SPC)/glycerol dioleate (GDO)-based LCNPs gives significantly better biocompatibility with a minimum of hemolytic activity and

Received: February 21, 2012
Accepted: April 19, 2012
Published: April 19, 2012

lipid mixing.[8] Depending on the composition, for example, the SPC/GDO ratio, this system can form reversed micellar cubic (I_2) and reversed hexagonal (H_2) phases, or intermediates or mixtures thereof, in equilibrium with excess water.[9] These structures are readily dispersed into nanoparticles by mechanical mixing with an appropriate steric stabilizer such as polysorbate 80 (P80).[10] Recent in vitro and in vivo studies with SPC/GDO-based LCNPs have demonstrated excellent particle stability and potential applications as delivery systems for both sparingly soluble substances and degradation sensitive water-soluble drug peptides, with improved pharmacokinetic performance and efficacy demonstrated in vivo.[10,11]

The properties of nonlamellar LCNPs as delivery vehicles or surface-modifying systems are to a large extent controlled by the surface interaction. These can be manipulated by the surface and/or particle properties. The focus of this study is to reveal the effect of the surface properties and which fundamental forces control such an interaction. Here we have focused on the electrostatic interaction by manipulating the charge of the surface from negative to cationic as well as the hydrophobicity of the surface. The aim is to understand how the particles interact with and respond to different types of interfaces. With regard to cationic surfaces, chitosan has come to prominence for use in new targeted drug delivery systems.[12] For a delivery vehicle, colloidal stability is important to prevent the loss of materials through adsorption to the storage container. On the other hand, for a surface-modifying system, maximal adsorption would be desirable to enhance delivery of the encapsulated materials. To date, there have been only a very limited number of studies that have aimed to address this issue.[11,13−16] The aim of this work is thus to study the interfacial properties of SPC/GDO-based LCNPs and to examine the effect of both particle and interfacial properties on the adsorption and the subsequently formed interfacial layer. The 40/40/20 SPC/GDO/P80 formulation was chosen because of its colloidal stability, pharmacokinetic acceptability, loading capacity, and reproducibility. The adsorption of LCNP on model surfaces is here studied using in situ null ellipsometry, which allows for time-resolved monitoring of the mean optical layer thickness and the adsorbed amount. These parameters provide insights into the attachment and relaxation of the lipid nanoparticle upon adsorption at surfaces. In this work, we focus on the effects that surface chemistry, solution property, and particle size have on the interfacial behavior of LCNPs.

MATERIALS AND METHODS

Materials. Soy phosphatidylcholine (SPC) was purchased from Lipoid GmbH (Ludwigshafen, Germany) containing as major components phosphatidylcholine (>94%), lysophosphatidylcholine (<1.0%), triglycerides (<1%), and free fatting acid (<0.05%). Glycerol dioleate (GDO) was obtained from Danisco (Aarhus, Demark), containing as major components diglycerides (96%), monoglycerides (0.2%), and triglycerides (3.8%). Polyoxyethylene (20) sorbitan monooleate (P80) was purchased from Apoteksbolaget AB (Umeå, Sweden). Sterile water from B. Braun Medical AB (Bromma, Sweden) was used for the preparation of LCNP dispersions, and Milli-Q purified water (18 MΩ cm) was used for all other solutions. All other solvents and reagents were of analytical grade and were used as received.

Sample Preparation. Small LCNPs were prepared as described previously.[10] Nonaqueous preformulations were prepared by mixing appropriate amounts of lipids (SPC and GDO) and particle stabilizer (P80) in 10 wt % ethanol (EtOH) to facilitate mixing. In all experiments, the SPC/GDO ratio was 50/50 (w/w). The preformulation [35/35/20/10 (wt/wt) SPC/GDO/P80/EtOH] was placed on a roller mixer for >1 h until it was mixed completely and then dispersed in 95 wt % water. The aqueous dispersions were immediately sealed, shaken, and vortexed for >18 h on a mechanical mixing table at >300 rpm and room temperature (RT). To produce large particles, a fraction of the LCNP dispersion obtained after mechanical vortexing was further processed by heat treatment. Heat treatment was performed using a bench-type autoclave (CertoClav CV-EL, Certoclav Sterilizer GmbH, Traun, Austria). The sample bottles were fitted with needles to prevent pressure buildup, heated for 13 min to vent the entrapped air and to heat the autoclave, and then held at 125 °C (1.4 bar) for 20 min. The samples were then allowed to cool and stored at RT until their further use.

Bulk liquid crystalline phases were prepared by mixing appropriate amounts of SPC, GDO, and P80 (total lipid amount of ∼0.5−1 g) in 10 wt % ethanol to facilitate mixing. The samples were placed on a roller mixer for >1 h until they were mixed completely and dried in a vacuum desiccator for 24 h using $CaCl_2$ as a sorbent to remove ethanol. Nonaqueous lipid mixtures prepared in such a way contained <1 wt % ethanol, which was controlled by weighing samples before and after the drying procedure. To hydrate nonaqueous samples, the required amounts of water (5−50 wt % with respect to the total sample mass) were added; samples were immediately sealed and left to equilibrate at room temperature for at least 3 weeks before experiments. To achieve phase homogeneity, during equilibration hydrated samples were centrifuged with the sample containers alternately up and down several times at 1500*g*.

Dynamic Light Scattering (DLS). The particle size distributions were measured by dynamic light scattering (Zetasizer Nano ZS, Malvern Instruments Ltd., Worcestershire, U.K.), using disposable sizing cuvettes filled with 1 mL of a 0.5 wt % LCNP dispersion at 25 °C. Data were collected after equilibration for 2 min and averaged over 12 measurements. The refractive indices used for lipid particles and water were 1.48 and 1.33, respectively. The apparent hydrodynamic radius was thereafter calculated using the Stokes−Einstein relation assuming spherical particles. The particle size distributions were characterized by the intensity-averaged mean and polydispersity index, PdI.

ζ Potential. The surface charge of the particles was monitored by measuring the ζ potential (Zetasizer Nano ZS, Malvern Instruments) with the laser Doppler electrophoresis method, using disposable ζ cells with 1 mL of a 0.5 wt % LCNP dispersion at 25 °C. The ζ potential was calculated using the Smoluchowski approximation for dispersion in water with a viscosity of 0.8872 cP, a refractive index of 1.33, and a dielectric constant of 78.5.

Cryogenic Transmission Electron Microscopy (cryo-TEM). LCNP dispersions for electron microscopy were prepared in a controlled environment vitrification system (CEVS) to ensure a stable temperature and to prevent the loss of water during sample preparation. The climate chamber temperature was kept at 25−28 °C, and the relative humidity was kept close to saturation to prevent sample evaporation. The samples were prepared by placing 5 μL of a 5 wt % LCNP dispersion on lacey carbon-coated copper grids and gently blotted with filter paper to obtain a thin liquid film (20−400 nm) on the grid. Immediately after being blotted, the grids were rapidly plunged into liquid ethane at −180 °C to vitrify the water-rich samples to prevent the formation of ice crystals and to preserve the internal crystalline structure. The vitrified specimens were stored in liquid nitrogen (−196 °C) until measurements were taken. An Oxford CT3500 cryo-holder and its workstation were used to transfer the samples into the electron microscope (Philips CM120 BioTWIN Cryo) equipped with a postcolumn energy filter (Gatan GIF100). The acceleration voltage was 120 kV, and the working temperature was kept below −180 °C. The images were recorded digitally with a CCD camera under low-electron dose conditions.

Small Angle X-ray Diffraction (SAXD). Synchrotron SAXD measurements were performed on beamline I711 at MAX-lab (Lund University), using a Marresearch 165 mm CCD detector mounted on a Marresearch Desktop Beamline baseplate.[11,12] Bulk SPC/GDO/P80 water liquid crystalline samples were mounted between kapton windows in a steel sample holder at a sample−detector distance of

1252 mm. Diffractograms were recorded at 25 °C under high vacuum with a wavelength of 1.07 Å and a beam size of 0.25 mm × 0.25 mm at the sample. The typical exposure time was 3 min. The resulting CCD images were integrated and analyzed using Fit2D provided by A. Hammersley (http://www.esrf.fr/computing/scientific/FIT2D). Calibrated wavelengths and detector positions were used.

Surface Preparation. The substrates used throughout this work were silica surfaces prepared from polished silicon wafers (p-type, boron-doped, resistivity of 1−20 Ω cm) purchased from Linköping University (Department of Chemistry, IFM, Linköping University, Linköping, Sweden) and SWI (Semiconductor Wafer, Inc., Taiwan). Silicon substrate surfaces are extremely flat, highly reflective, and therefore ideal for ellipsometry measurements. These silicon substrates were thermally oxidized at ∼900 °C in an oxidation furnace to yield ∼300 Å of silicon oxide (in practice a silica surface). The silica surface is composed of silanol hydroxyl groups (Si-OH) with approximately five OH groups per nanometer,[2,17] such that the surface chemistry could be easily modified. To investigate the effect of surface properties on adsorption, the silica surfaces were made hydrophobic and positively charged by reaction with different silanes.

The oxidized substrates were cut into small slides with a width of ∼10 mm. Before being used, the substrates were cleaned first in a base mixture of 25% NH_4OH (pro analysi, Merck), 30% H_2O_2 (pro analysi, Merck), and H_2O (1/1/5, by volume) at 80 °C for 5 min, and rinsed with water, followed by an acid mixture of 32% HCl (pro analysi, Merck), 30% H_2O_2, and H_2O (1/1/5, by volume) at 80 °C for 5 min. The substrates were then thoroughly rinsed with water and then ethanol and stored in ethanol (>99%) until further use. Immediately before each measurement, the substrates were rinsed with ethanol and water, dried with N_2 gas, and then plasma cleaned (Harrick Scientific Corp., model PDC-3XG) for 5 min.

The hydrophobic silica surfaces were prepared by gas-phase silanization. Immediately before silanization, the silicon wafers were plasmas cleaned for 5 min in air (0.04 mbar) to remove any organic contaminants and then placed in a desiccator with approximately 1 mL of dimethyloctylchlorosilane (DMOCS, Fluka). The desiccator was then evacuated with a vacuum pump for over 20 min (about 0.01 mbar), and left overnight at room temperature. The next day, the silanized substrates were sonicated in tetrahydrofuran (THF) and then in ethanol for 20 min to remove any unreacted materials. The hydrophobized silica were then stored in ethanol until further use.

The cationic silica surfaces were prepared by liquid-phase silanization. Plasma-cleaned silica substrates were dried in an oven to remove any residual water moisture. The substrates were then incubated in anhydrous toluene with 2% 3-aminopropyltriethoxysilane (APTES, Fluka) under a nitrogen atmosphere for approximately 2 h. The silanized substrates were then sonicated in toluene, a toluene/ethanol mixture (1/1), and ethanol to remove any unreacted materials. The cationic substrates were then dried at 120 °C and stored in ethanol until further use.

The chitosan-coated surfaces were prepared by adsorbing chitosan in water to the plasma-cleaned silica surface. Chitosan (Fluka) was dissolved in 1 vol % acetic acid (10 mg/mL) for 24 h with continuous stirring until complete dissolution. The dissolved chitosan solution was then further diluted with water to a concentration of 1 mg/mL. The coating of chitosan onto the silica was monitored in real time with ellipsometry via injection of 500 μL of the chitosan stock solution into the ellipsometry cuvette to a final concentration of 0.1 mg/mL. The chitosan coating was completed when the adsorbed thickness and amount reached an equilibrium value. The chitosan-coated substrates were then used immediately.

Ellipsometry. The adsorption measurements were monitored in situ by null ellipsometry as described previously.[18,19] The instrument used was an automated thin-film null ellipsometer (type 43603-200E, Rudolph Research) with a xenon arc lamp light source filtered to select a wavelength of 4015 Å. The substrate was placed inside a 5 mL trapezoid cuvette with a thin glass window made from a glass coverslip. The sample cell was thermostated to 25 °C and agitated with a magnetic stirrer. Measurements were taken with an angle of incidence of ∼67.85°.

Before each experiment, the silica surface properties were determined using a three-layer substrate model, assuming bulk isotropic silicon with a thin layer of oxide in an ambient medium. The complex refractive index of the bulk silicon substrate ($N_2 = n_2 - jk_2$) and the thickness and refractive index of the oxide layer were determined by measuring the ellipsometric angles (ψ and Δ) in air and liquid environments and averaged over four different zones to cancel out effects of optical imperfections in the components of the apparatus.

By monitoring the change in the amplitude and phase of the reflected light, we can model the optical thickness (d) and refractive index (n) of an additional adsorbed layer, according to an optical four-layer model. The absorbed amount, Γ, then can be calculated using de Feijter's approximation[20]

$$\Gamma = \frac{(n - n_0)d}{\mathrm{d}n/\mathrm{d}c}$$

where n_0 is the refractive index of the solvent and $\mathrm{d}n/\mathrm{d}c$ is the refractive index increment of the adsorbed materials as a function of its bulk concentration. The refractive index increment value ($\mathrm{d}n/\mathrm{d}c$ = 0.15 mL/g) was measured from aqueous solutions with different LCNP concentrations using a Multiscale Automatic refractometer (RFM-81, λ = 5893 Å, BS, Tunbridge Wells, England).

After the surface had been characterized, measurements were conducted by injecting a small aliquot of the concentrated LCNP dispersion (5 wt %, 50 mg/mL) into the cuvette to a final concentration of 0.1 mg/mL.

RESULTS

Formation and Characterization of LCNPs. LCNPs were prepared by mechanical vortexing of the liquid crystalline-forming lipid mixtures with P80 as the stabilizer and optionally followed by heat treatment (see above). The size distributions of the LCNP dispersion were measured via DLS (Figure 1).

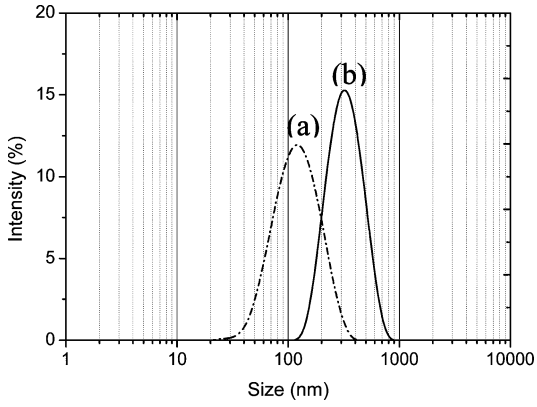

Figure 1. Particle size distribution of SPC/GDO/P80 LCNPs dispersed in 95% water by being shaken overnight at 300 rpm (a) and then treated with heat (b).

The particles obtained after mechanical shaking had a mean diameter of 111 nm with a PdI of 0.2 (Table 1). Heat treatment of these particles increased the particle size (d = 300 nm) and narrowed the size distribution (PdI = 0.1). High-resolution cryo-TEM images confirmed the size distribution observed by DLS (Figure 2).

Figure 2 shows the cryo-TEM images of the SPC/GDO/P80 nanoparticles before and after heat treatment. Without heat treatment, a relatively polydisperse mixture of LCNPs was produced, and vesicular aggregates are also present (Figure 2a). The heat treatment induced fusion of these aggregates with a more uniform particle size distribution (Figure 2b). The cryo-

Table 1. Mean Particle Diameters (d), Polydispersity Indices (PdI), and ζ Potentials of SPC/GDO/P80 LCNPs before and after Heat Treatment in Water (pH 5.5) and 0.1 mM HCl (pH 4)

pH	d (nm)	PdI	ζ potential (mV)
	Before Heat Treatment		
4	107 ± 1	0.18	−5.5 ± 0.2
5.5	111 ± 1	0.21	−14.6 ± 0.4
	After Heat Treatment		
4	300 ± 2	0.13	0.0 ± 0.1
5.5	300 ± 4	0.14	−9.2 ± 0.4

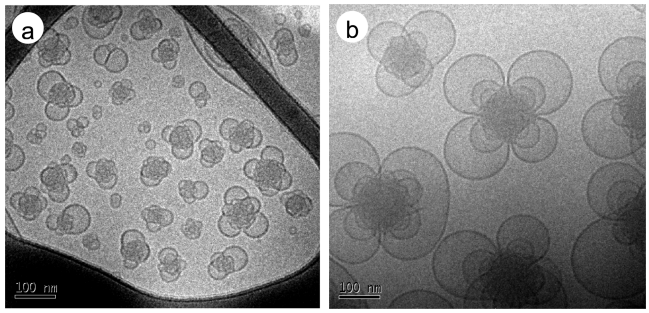

Figure 2. Cryo-TEM images of SPC/GDO/P80 LCNPs (a) before and (b) after heat treatment.

TEM images show that the LCNPs have an inner denser core surrounded by an outer petal-like shell of vesicles, presumably enriched with the P80 stabilizer. Visual judgment of the denser inner core suggests the presence of a complex disrupted liquid crystalline structure.

The internal nanostructure of the SPC/GDO/P80 (40/40/20, by weight) LCNPs was further characterized using SAXD. Because the diffraction pattern for the LCNPs was too weak be resolved, the corresponding bulk liquid crystalline phases of the same lipid composition were prepared at lower hydration levels. Figure 3a compares the SAXD data of the fully hydrated (50 wt % water) SPC/GDO (50/50) and SPC/GDO/P80 (40/40/20) mixtures. These data show that SPC/GDO without P80 form a reversed micellar cubic phase (I_2) in the *Fd*3*m* space group, which is apparent from the location of the first nine Bragg peaks at relative positions at a $\sqrt{3}/\sqrt{8}/\sqrt{11}/\sqrt{12}/\sqrt{16}/\sqrt{19}/\sqrt{24}/\sqrt{27}/\sqrt{32}$ q ratio. On the other hand, SPC/GDO/P80 mixtures show only one sharp Bragg peak located at q = 0.48 nm^{-1} and two broad diffraction peaks at q values of approximately 0.92 and 1.70 nm^{-1}. These data do not allow an unambiguous determination of the liquid crystalline phase(s); therefore, a series of samples with different degrees of hydration with 5−50 wt % water were investigated, and the resulting diffractograms are shown in Figure 3b. At water contents of ≤15 wt %, a reversed hexagonal phase (H_2) that is characterized by three distinctive reflections at a relative q position ratio of $1:\sqrt{3}:2$ is formed. At higher levels of hydration, this phase transforms into a lamellar phase (L_α) showing the typical appearance of Bragg peaks at relative q positions in ratios of 1, 2, and 3. With an increasing water content, a lamellar repeat distance increases from ∼8 nm at 25 wt % water to almost 14 nm at 50 wt % water. As also seen from Figure 3b, the diffractograms for the H_2 and L_α phases observed at limited and full hydration, respectively, contain an additional broad diffraction peak located at q values of approximately 0.8−0.9 nm^{-1} that can be attributed to a

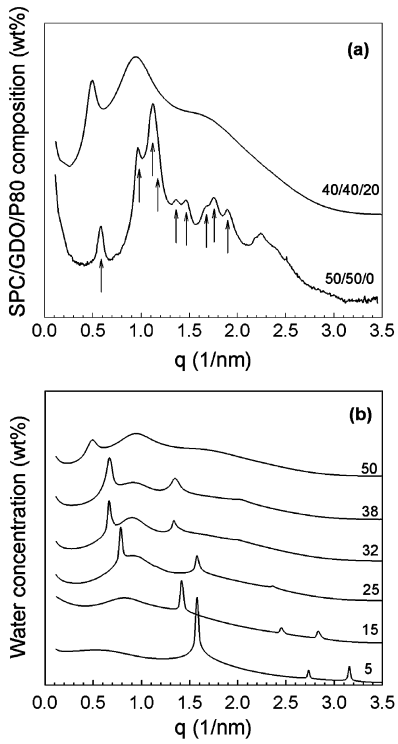

Figure 3. (a) SAXD patterns of the fully hydrated (50 wt % water) nondispersed SPC/GDO (50/50) and SPC/GDO/P80 (40/40/20) mixtures. Arrows show indexing of the reversed micellar cubic phase of the *Fd*3*m* space group. (b) SAXD data of the SPC/GDO/P80 (40/40/20) mixture from limited hydration at 5 wt % water to fully hydrated at 50 wt % water. All measurements were performed at 25 °C.

reversed micellar solution phase (L_2). The observed q value would correspond to some average spacing between reversed micelles of 7−8 nm. The SAXD data on the swelling behavior and the comparison with the data in the absence of P80 reveal that the SPC/GDO/P80 formulation used in this study forms a mixture of L_α and L_2 phases under full hydration conditions. From the combined SAXD and cryo-TEM results, we can conclude that the core of the LCNP particles has a high lipid content with disordered liquid crystalline structure, most likely L_2, while the shell is more swollen with water, with the outer part comprising lamellar structure providing colloidal stability.[3,4]

To improve our understanding of the interfacial properties of the SPC/GDO/P80 nanoparticles, the surface charges of the nanoparticles were estimated by measuring the ζ potential (Table 1). The particles have a negative charge (−14 mV) that decreases with a decrease in pH. The origin of the negative charge is likely the presence of small amounts of free fatty acids in the lipids and stabilizer[3] and the preferential adsorption of hydroxyl group at the oil−water interface.[16] Free fatty acids, such as oleic acid, have a pK_a of ∼5 and are therefore expected to be 90% protonated at pH 4, which would explain the near-zero ζ potential measured at pH 4. Here it should be noted that the apparent pK_a is affected by a range of environmental factors such as the density of fatty acids and the type of self-assembled structure.[21] However, in the studied LCNP dispersions, we expect a low concentration of fatty acid, and hence, the pK_a is close to that of the free fatty acid. The heat treatment of the particles did not appear to significantly affect the overall surface

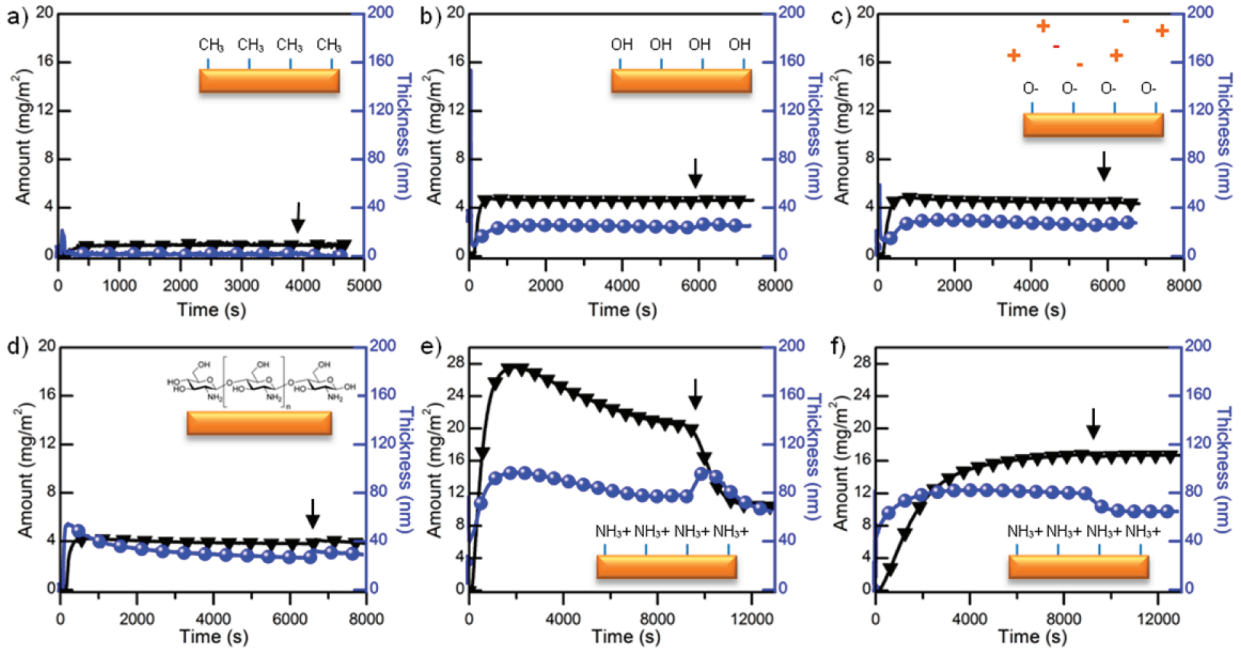

Figure 4. In situ null ellipsometry data of the adsorbed amount (▼) and layer thickness (●) as a function of time after addition of 0.1 mg/mL small 111 nm SPC/GDO/P80 LCNPs on (a) hydrophobic DMOCS_Si in water, (b) hydrophilic Si in pH 4 water, (c) hydrophilic Si in salt water (0.1 M NaCl and 0.017 M $CaCl_2$), (d) chitosan-coated Si in water, (e) cationic APTES_Si in water, and (f) cationic APTES_Si in pH 4 water. The arrows indicate when rinsing with pure solvent occurred.

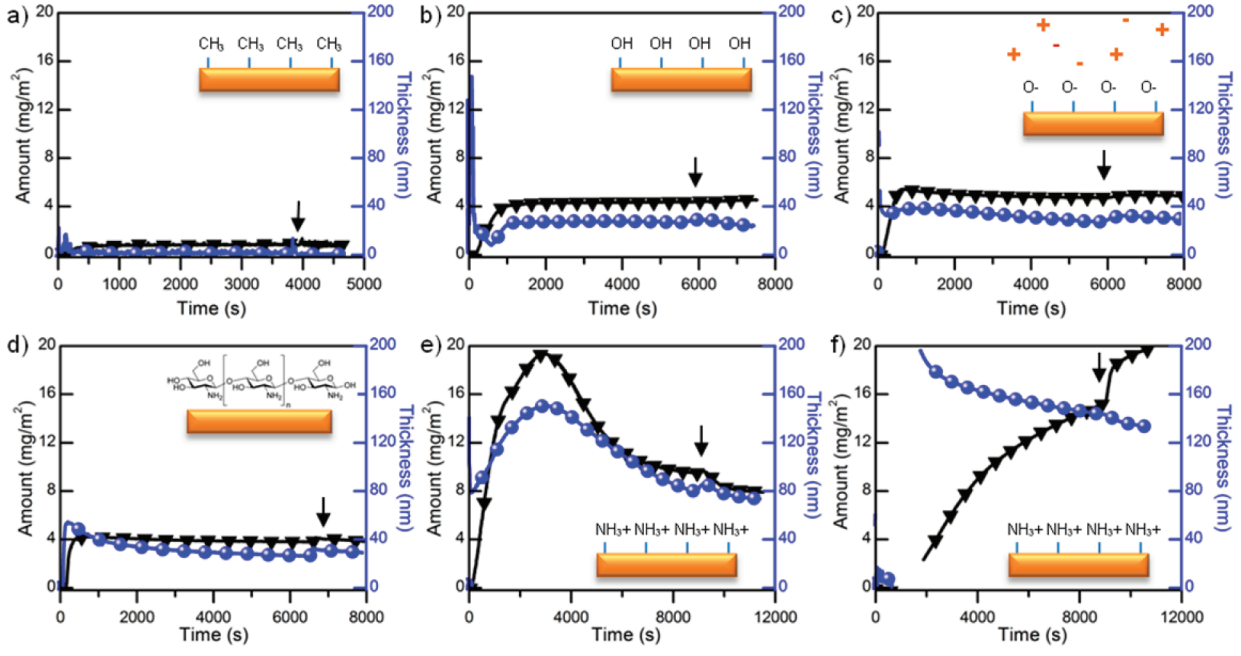

Figure 5. In situ null ellipsometry data of the adsorbed amount (▼) and layer thickness (●) as a function of time after addition of 0.1 mg/mL large 300 nm SPC/GDO/P80 LCNPs on (a) hydrophobic DMOCS_Si in water, (b) hydrophilic Si in pH 4 water, (c) hydrophilic Si in salt water (0.1 M NaCl and 0.017 M $CaCl_2$), (d) chitosan-coated Si in water, (e) cationic APTES_Si in water, and (f) cationic APTES_Si in pH 4 water. The arrows indicate when rinsing with pure solvent occurred.

charge. The ζ potentials of the particles after heat treatment were very similar.

Adsorption of LCNPs at the Hydrophobic Surface. Adsorption of LCNPs at the hydrophobic DMOCS-silanized silica surface was monitored in situ using null ellipsometry. Results show a rapid adsorption reaching a maximal adsorbed amount and layer thickness of 1 mg/m^2 and 1−2 nm, respectively, within a few minutes (Figures 4a and 5a). The resulting adsorption properties were basically independent of the initial particle size and consistent with what is expected for a lipid monolayer of SPC, GDO, and P80. This observation is in agreement with the previous study of GMO-based cubic crystalline nanoparticles showing monolayer adsorption at the hydrophobic interface.[19]

Adsorption of LCNPs on the Silica Surface. Adsorption of LCNPs on the hydrophilic silica surface is dramatically

dx.doi.org/10.1021/am300301b | ACS Appl. Mater. Interfaces 2012, 4, 2643−2651

different from that on hydrophobic surfaces. Panels b and c of Figures 4 and 5 show the adsorption of small (111 nm) and large (heat-treated, 300 nm) SPC/GDO/P80 nanoparticles on silica, respectively. Notably, the LCNPs only adsorbed at a physiological concentration of salt (0.1 M NaCl and 0.017 M $CaCl_2$) or at a low pH (pH 4), while no detectable adsorption was measured in pure water at pH 5.5. This is consistent with both particles and silica surfaces being negatively charged at pH 5.5, resulting in a net electrostatic repulsion between the particles and the surface at higher pH values, i.e., pH >5, consistent with a previous study of GMO-based LCNPs at silica.[22] The silica surface has an isoelectric point (iep) at pH ~2. Above the iep, the negative surface charge depends strongly on the pH and salt concentrations.[23] The addition of 0.1 mM HCl lowered the pH of the water from pH 5.5 to 4, where the surface charge density of silica is very low.[23] This decrease in pH resulted in a notable adsorption increase of LCNPs from zero at pH 5.5 to an adsorbed amount at steady state of 4 mg/m^2 and a thickness of ~25 nm for both LCNP fractions at pH 4 (Figures 4b and 5b). Interestingly, for both small and large LCNPs, a transition from quite large initial adsorbed layer thicknesses through a transient minimum is observed before steady state values are obtained. The transition period is slightly shorter during adsorption of LCNPs with a smaller mean particle size, as may be expected after consideration of diffusion and relaxation.

Adsorption of LCNPs on Cationic Surfaces. An important driving force for particle adsorption may be electrostatic attractive interaction between LCNPs and the oppositely charged surfaces. For this purpose, two types of cationic surfaces were prepared; chitosan-coated surface and APTES-silanized silica surface. Chitosan is a linear polysaccharide composed of D-glucosamine and *N*-acetyl-D-glucosamine, naturally found in chitin of the exoskeleton of sea crustaceans. The amino group in chitosan has a pK_a of approximately 6.5,[24] which makes it slightly positively charged at the pH values used in this experiment (pH 5.5). Chitosan was adsorbed to the silica surface from a 0.1 mg/mL solution in water for >1 h to reach a steady state adsorbed amount of ~0.5 mg/mL with a thickness of 5−20 Å. The adsorbed amount is similar to previously observed values for adsorption of chitosan on silica.[15] The SPC/GDO/P80 LCNPs were then added to the solution and allowed to adsorb at the chitosan-coated surface. The resulting adsorption curves show that the chitosan-coated surface promotes adsorption of the LCNPs in water, with a steady state surface excess of ~3−4 mg/m^2 and a layer thickness of ~30 nm (Figures 4d and 5d and Table S1 of the Supporting Information). This is reasonably similar to the adsorption of LCNP on silica at pH 4 or in presence of salt at pH 5.5 (Figures 4b,c and 5b,c). Clearly, the positively charged chitosan-coated surface promotes the attachment of the particles, but adsorption is fairly weak because of the relatively low excess charge of chitosan. To effectively increase the charge density of the surface, the silica surface was chemically functionalized with a positively charged silane, APTES, creating a cationic surface with a high charge density. The APTES-silanized silica surface presents a monolayer of primary amine on the surface where the pK_a of the amino group is around 11,[25] making it highly positively charged under the experimental conditions used in this study (pH 4 and 5.5).

As expected, adsorption of LCNPs on the APTES-silanized silica was dramatically different from that on bare silica or chitosan-functionalized surfaces. A very thick LCNP layer is observed at the APTES-silanized silica with final adsorbed amounts of the different LCNP fractions after rinsing at steady state of 8−10 and 16−20 mg/m^2 at pH 5.5 and 4, respectively (Figures 4e,f and 5e,f). The measured adsorption kinetics was pH-dependent, which may be due to the difference in surface charge of the LCNPs. In pure water (pH 5.5), the nanoparticles were more negatively charged than at pH 4. In line with the stronger electrostatic attraction, LCNPs showed a more rapid initial adsorption in pure water at pH 5.5 versus that in acidic water at pH 4 (Table S1 of the Supporting Information). In pure water, the adsorbed amount increased proportionally with time, and after ~1 h, the adsorbed amount reached a maximum of ~20−26 mg/m^2. At the same time, the layer thickness also reached peak values corresponding to approximately 81 and 62% of the hydrodynamic diameter of the small and large nanoparticles, respectively. After reaching maxima, both the adsorbed amount and layer thickness showed a slow decay over time. These kinetic features of the adsorption process appear consistently for both small and large particles and may reflect transient restructuring of the nanoparticles at the interface. One hypothesis is that the strong attractive force between the nanoparticles and the surface results in a relaxation deformation of the particles, resulting in a decrease in the adsorbed thickness. The kinetics of adsorption of LCNPs on an APTES-silanized silica surface was much slower at pH 4, which shows the influence of attractive interactions on adsorption (Figure 6). As the LCNPs are less negatively charged, the strength of the attractive interaction is lower. The adsorption profile of larger LCNPs showed the formation of a relatively thick (>150 nm) layer, even though the layer thickness decreased slightly during the continued buildup (Figure 5f). This observation suggests direct adsorption of intact nanoparticles, which may be further compacted and/or spread at the surface over time. It should be noted that the current measurement setup cannot accurately distinguish a layer thickness of >200 nm because of the cyclicity of ψ and Δ determined by ellipsometry, which is why the initial part of the adsorption curve cannot be shown.

DISCUSSION

This study shows how surface chemistry and solvent conditions can be used to control the adsorption of lipid LCNPs at interfaces (Figure 6). The adsorption curves (Figures 4 and 5) demonstrate the evolution over time of the adsorbed amount and the layer thickness on different surfaces. As expected, the largest adsorption was observed on the highly charged cationic surface, where the solution pH greatly affected the adsorption kinetics and also the final adsorbed amount (Figure 6 and Table S1 of the Supporting Information). The adsorption behavior can be classified into three different types depending on the LCNP surface interaction: (1) very strong adsorption and thick layer structures (>8 mg/m^2 and >60 nm, respectively) on highly charged cationic surfaces, (2) thick multilayer structures (4−6 mg/m^2 and 20−35 nm, respectively) on hydrophilic weakly charged surfaces, and (3) mixed monolayers of lipids (<1 mg/m^2 and 1−2 nm, respectively) on hydrophobic surfaces. The results suggested that the hydrophobic attractive interaction between the lipids and the surface completely disrupts the LCNP structure at hydrophobic surfaces, resulting in the formation of a single monolayer of lipids at the surface that prevents further adsorption. In contrast, LCNPs appear to adsorb relatively intactly on highly charged cationic surfaces, resulting in a surface structure composed of individual particles. On hydrophilic weakly charged surfaces such as silica and

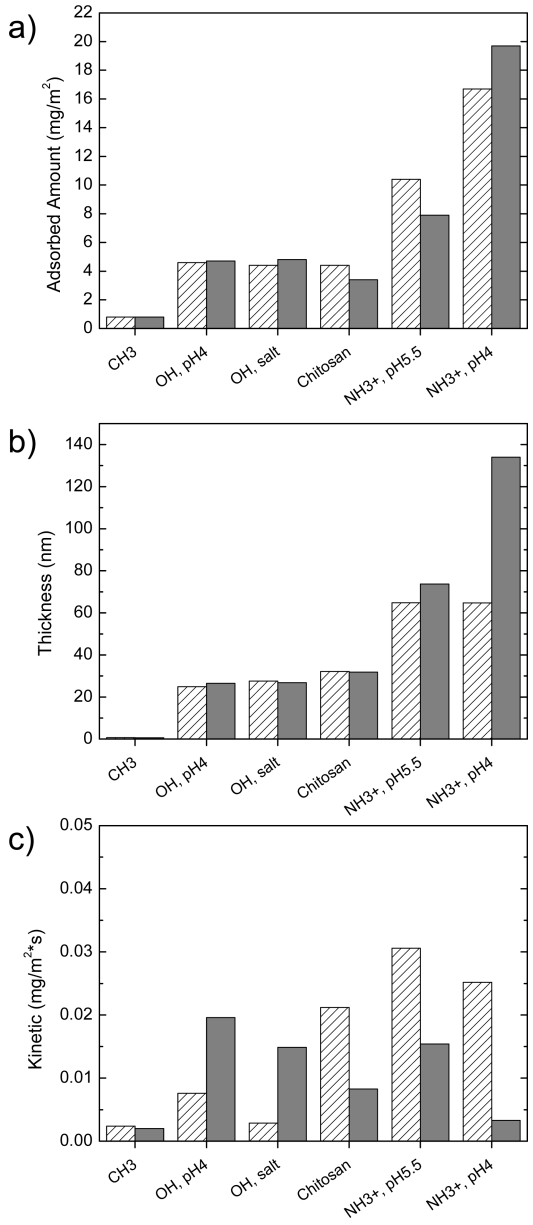

Figure 6. Adsorbed amount (a), layer thickness (b), and initial adsorption kinetics (c) of small (striped bars) and large (gray bars) SPC/GDO/P80 LCNPs on surfaces with different surface chemistries and/or solvent conditions.

chitosan-coated silica, intermediate multilayer structures are observed.

The mechanism of interaction of LCNPs and the substrate surfaces depends on the substrate chemistry. On the hydrophobic surface, hydrophobic attraction between the substrate surface and the hydrophobic lipid tail results in monolayer coverage. On the cationic surface, electrostatic interaction between the negatively charged LCNPs and the positively charged surface becomes the main driving force for adsorption. In this study, we also showed that the solution pH can greatly affect the adsorption kinetics and at the same time restructure the adsorbed particle layer. On the hydrophilic weakly charged silica surface, we have shown that P80 is adsorbed on the silica surface at low pH, which has also been shown previously.[26] The mechanism for adsorption arises from the nonelectrostatic affinity between the polymer and silica. More specifically, the adsorption may arise from polyethylene glycol (PEG) units on P80 and the silanol group on the silica surface. Adsorption of PEG or a PEG-containing polymer on silica has been extensively studied,[27−29] and the nonelectrostatic attraction is thought to originate from the formation of a hydrogen bond between the ethoxy units in the polymer and the silanol (Si-OH) group on the surface,[29,30] although our view is that hydrophobic interactions between PEG segments and more hydrophobic siloxane (Si-O-Si) groups on the silicon oxide surface[17] play an important role. It should be noted that the ratio of silanol to siloxane groups can be manipulated by the surface treatment.[17] Similar to our current observation, the nonelectrostatic affinity between PEG and silica is very sensitive to solution pH and decreases sharply with an increase in pH. These observations suggest that adsorption of SPC/GDO/P80 LCNPs on a silica surface is mainly driven by the nonelectrostatic affinity between PEG chains of P80 and silica. The origin of the nonelectrostatic affinity may be the combination of formation of a hydrogen bond between the silica surface and the ethoxy units and the hydrophobic interaction between the PEG segments and siloxane groups.

Particle size did not appear to have a strong influence on the final layer properties after preadsorbed layers at weakly charged surfaces had been rinsed with lipid free solutions (Figure 6). Independent repeated measurements showed a reproducible adsorbed amount and layer thickness with <15% variation. However, very significant effects of particle size on the final layer thickness can be seen at the cationic APTES-silanized silica surface, where the thickness of the layer formed by the larger LCNPs is approximately twice as large as the corresponding layer formed by smaller LCNPs (Figure 6b). The adsorption behavior on the cationic surface is very sensitive to the surface charge and particle size, such that comparisons were made in the same batch of functionalized surfaces and particles. For both larger and smaller LCNPs, the layer thickness after rinsing was approximately half the size of the mean particle hydrodynamic diameter. One should note that the calculated layer thickness in ellipsometry is the mean optical thickness based on a homogeneous layer model, where lateral inhomogeneities are not taken into account.[31] The measured ellipsometry thickness is by definition smaller than the particle hydrodynamic diameter, in particular when the surface coverage is low.[19] The LCNPs can also become flattened when adsorbed on surfaces. Previous AFM measurements revealed that the adsorbed LCNPs are slightly flattened[32] but intact on the surface. A fluorescence microscopy study further showed no lateral organization of the particles.[22]

To quantify and gain further insight into the adsorption process, the initial rate of adsorption was extracted from the slope of the initial adsorption curve (Figure 6c). The theoretical adsorption rate ($d\Gamma/dt$) was calculated on the basis of the kinetic model assuming that the adsorption is determined by mass transport to the surface. The mass transport in the used cuvette geometry can be described as being controlled by diffusion from a bulk of constant concentration because of the agitation across a stagnant (unstirred) layer of solvent of thickness δ, where the initial mass transfer rate, $d\Gamma/dt$ (adsorption rate), is solely controlled by the diffusion that is proportional to the bulk concentration, C, as $d\Gamma/dt = CD/\delta$, where D is the diffusion coefficient.[33] For our setup and experimental conditions, δ assumes a value of 100 μm from the surface as discussed in a previous study for the ellipsometry setup used in this work.[34] The expected diffusion-controlled

adsorption rates of the LCNPs, assuming spherical particles using the Stokes–Einstein equation to calculate the diffusion constant (D) at 0.1 mg/mL, were approximately 4×10^{-4} and 1.6×10^{-4} mg m^{-2} s^{-1} for 111 and 300 nm particles, respectively. The measured initial adsorption rates on hydrophilic silica surfaces are 2 orders of magnitude greater than the theoretical values, 1×10^{-2} and 2×10^{-2} mg m^{-2} s^{-1} for small and large LCNPs, respectively (Figure 6c). This suggests that preferential adsorption of the smaller aggregates or free polymers may have dominated the initial adsorption.

To reveal the effect of a free stabilizer, P80, in the solution on the adsorption of LCNPs, we studied the adsorption of the neat stabilizer on the hydrophobic, hydrophilic, and cationic surfaces. The results show that P80 forms thin layers of submonolayer thickness on the hydrophobic surface and bilayer type of adsorbed layers with a thickness of ∼4 nm on the hydrophilic and cationic surfaces (Table 2). The initial adsorption rate of free P80 stabilizer on the hydrophilic and cationic surfaces was on the same order of magnitude as that observed with the nanoparticles (Table 2). These findings imply initial adsorption of the free highly water-soluble P80 stabilizer on the surfaces. To isolate the effect of the stabilizer on particle adsorption, the surfaces were preadsorbed with P80 before the introduction of the particles. The P80 bilayer on the surface dramatically reduces the adsorption of LCNPs (see Figure S3 of the Supporting Information). On the hydrophilic surface, addition of LCNPs on the preadsorbed P80 bilayer produces an initial rapid increase in thickness that quickly returns to the bilayer thickness. The dynamic adsorption process suggests attachment of LCNPs followed by possible lipid–surfactant exchange, which leads to detachment of the particles. A similar phenomenon has also been observed for GMO-based LCNPs interacting with a supported lipid bilayer consisting of dioleoylphosphatidylcholine (DOPC).[14] The adsorption of a free stabilizer can affect the adsorption of LCNPs but could not solely explain the interfacial behavior.

Table 2. Adsorbed Amounts, Layer Thicknesses, and Initial Adsorption Kinetics of LCNPs and the Individual Components (SPC, GDO, and P80) on Hydrophobic (CH_3), Hydrophilic (OH), and Cationic (NH_3^+) Surfaces[a]

substrate	pH	materials	amount (mg/m^2)	thickness (nm)	initial kinetics (mg m^{-2} s^{-1})
CH_3	5.5	SPC/GDO/P80 LCNPs	0.8 ± 0.12	0.6 ± 0.3	0.0020
CH_3	5.5	P80	1.8 ± 0.04	0.9 ± 0.1	0.0152
CH_3	5.5	SPC	2.9 ± 0.01	61.0 ± 0.1	0.0013
CH_3	5.5	GDO	0.4 ± 0.02	2.3 ± 0.9	0.0001
OH	4	SPC/GDO/P80 LCNPs	4.7 ± 0.01	26.5 ± 0.2	0.0196
OH	4	P80	2.6 ± 0.03	4.0 ± 0.2	0.0111
OH	4	SPC	4.0 ± 0.01	15.9 ± 0.3	0.0020
OH	4	GDO	no adsorption		
NH_3^+	4	SPC/GDO/P80 LCNPs	19.7 ± 0.06	134.0 ± 0.2	0.0033
NH_3^+	4	P80	1.4 ± 0.01	4.7 ± 0.3	0.0072
NH_3^+	4	SPC	no adsorption		
NH_3^+	4	GDO	no adsorption		

[a]The mean values ± standard deviations of measurement errors at steady state after rinse are presented.

The adsorbed bilayer thickness was only fractions (14%) of the observed layer thickness of multilayer dimensions observed for adsorption of LCNPs on silica, which indicates that adsorption of nanoparticles also took place. A similar reduction in the amount of particle adsorption is also observed on the cationic surface that is precoated with P80. Comparison between the adsorption of LCNPs on a cationic surface and one with preadsorbed P80 using the same surface and particle showed a 55% reduction in the adsorbed amount and a 20% reduction in the layer thickness. In fact, a similar competition between the adsorption of the stabilizer and the intact particles was also observed for the GMO-based LCNPs, which are stabilized by Pluronics F127 PEO-PPO-PEO triblock copolymer.[22]

The cryo-TEM images of LCNPs clearly show the presence of lamellar structure surrounding the particle surface. The presence of such a lamellar shell is expected to largely influence the adsorption behavior of the LCNPs. Comparison of the adsorption behavior of a simple aqueous dispersion of the lamellar phase, liposomes, and the more complex LCNPs studied here can therefore shed light on the adsorption mechanism of the LCNPs. Liposomes have been extensively used to form supported lipid bilayers on hydrophilic surfaces.[35−38] The formation of a supported lipid bilayer from vesicle fusion rests on the fact that the phospholipids are more likely to form a flat bilayer than a curved one on the vesicle. When a spherical vesicle is deposited on a surface, depending on the surface properties and vesicle stability, the vesicles could burst and spread into a bilayer structure on the surface. The transition from intact vesicle adsorption to supported bilayer formation depends strongly on the vesicle–surface and vesicle–vesicle interactions.[36,38] Similar to vesicle adsorption, the adsorption of LCNPs on surfaces is also dictated by the particle–surface interaction, but with the added complexity that the outer lamellar shell is enriched with P80 steric stabilizer and that the core of the LCNPs is likely to be more viscous. Both factors are expected to hamper the spreading of the LCNPs unless the particle surface interaction is sufficiently strong. Therefore, we observed complete spreading of the LCNPs only on the hydrophobic surface. Unlike the transformation from vesicle to bilayer on the hydrophilic silica surface, adsorption of LCNPs, as shown earlier, leads to formation of a significantly thicker layer. Adsorption of only P80 stabilizer on the hydrophilic and cationic surface showed formation of a simple bilayer structure with a layer thickness of ∼4 nm. This confirms the affinity of the stabilizer for the hydrophilic surface, which, in part, leads to adsorption of LCNPs.

LCNPs have great potential as drug carriers; however, surprisingly little is known about the interfacial behavior of LCNPs on surfaces. The majority of the literature has investigated the GMO-based LCNP.[11,13−16,22] In this study, we examine for the first time the interfacial behavior of SPC/GDO/P80 LCNPs on surfaces. The novel SPC/GDO/P80 system has high drug loading capability, excellent stability, improved pharmacokinetics, and limited hemolytic activity.[8,10] These LCNPs have the potential to be an improved alternative to current emulsion products.[10] This study considered one LCNP formulation, and the observed adsorption of these nanoparticles on hydrophobic, hydrophilic, and charged surfaces. Depending on the interfacial chemistry and solvent conditions, a varying adsorption response was observed. This further suggests that it may be possible to alter the adsorption interaction by simply changing the particle formulation. The relatively high concentration (20%) of P80 stabilizer was

chosen for the ease of dispersion. Further knowledge of LCNP surface interaction as a function of lipid composition and different stabilizer concentrations is indeed of great interest and is addressed in a just completed study.[39]

CONCLUSION

In this work, we studied the adsorption of lipid liquid crystalline nanoparticles on surfaces as a function of the surface properties. The effects of surface chemistry and solvent conditions were found to greatly influence particle adsorption. On a hydrophobic surface, strong hydrophobic interaction results in disintegration of lipid particles and formation of a lipid monolayer. On a hydrophilic silica surface, a thicker multilayer was formed in the presence of salt or low pH. On a cationic silanized silica surface, electrostatic attraction between the negatively charged particle and the positively charged surface results in the adsorption of intact crystalline particles at high concentrations. The adsorption behavior depends on the intricate balance between the individual components of LCNPs and the substrate surface. The adsorbed amount and resulting layer structure are determined by the electrostatic particle−surface interaction as well as the nonelectrostatic affinity between the polymer and surface.

ASSOCIATED CONTENT

Supporting Information

Additional observations. This material is available free of charge via the Internet at http://pubs.acs.org.

AUTHOR INFORMATION

Corresponding Author

*E-mail: debby.chang@fkem1.lu.se.

Notes

The authors declare no competing financial interest.

ACKNOWLEDGMENTS

This work was financially supported by Swedish Foundation for Strategic Research. We thank Bengt Jonsson at Lund University for valuable discussions, Camilla Cervin at Camurus for the introduction to particle preparation, and Gunnel Karlsson at the Biomicroscopy Unit at Lund University for technical assistance with cryo-TEM.

REFERENCES

(1) Drummond, C. J.; Fong, C. *Curr. Opin. Colloid Interface Sci.* **1999**, *4*, 449−456.
(2) Lawrence, M. J. *Chem. Soc. Rev.* **1994**, *23*, 417−424.
(3) Barauskas, J.; Johnsson, M.; Johnson, F.; Tiberg, F. *Langmuir* **2005**, *21*, 2569−2577.
(4) Barauskas, J.; Johnsson, M.; Tiberg, F. *Nano Lett.* **2005**, *5*, 1615−1619.
(5) Boyd, B. J.; Dong, Y. D.; Rades, T. *J. Liposome Res.* **2009**, *19*, 12−28.
(6) Gustafsson, J.; Ljusberg-Wahren, H.; Almgren, M.; Larsson, K. *Langmuir* **1996**, *12*, 4611−4613.
(7) Gustafsson, J.; Ljusberg-Wahren, H.; Almgren, M.; Larsson, K. *Langmuir* **1997**, *13*, 6964−6971.
(8) Barauskas, J.; Cervin, C.; Jankunec, M.; Spandyreva, M.; Ribokaite, K.; Tiberg, F.; Johnsson, M. *Int. J. Pharm.* **2010**, *391*, 284−291.
(9) Oradd, G.; Lindblom, G.; Fontell, K.; Ljusbergwahren, H. *Biophys. J.* **1995**, *68*, 1856−1863.
(10) Tiberg, F.; Johnsson, M.; Barauskas, J.; Norlin, A. *J. Nanosci. Nanotechnol.* **2006**, *6*, 3017−3024.
(11) Cervin, C.; Vandoolaeghe, P.; Nistor, C.; Tiberg, F.; Johnsson, M. *Eur. J. Pharm. Sci.* **2009**, *36*, 377−385.
(12) Patel, M. P.; Patel, R. R.; Patel, J. K. *J. Pharm. Pharm. Sci.* **2010**, *13*, 536−557.
(13) Dong, Y. D.; Larson, I.; Bames, T. J.; Prestidge, C. A.; Boyd, B. J. *ACS Appl. Mater. Interfaces* **2011**, *3*, 1771−1780.
(14) Vandoolaeghe, P.; Rennie, A. R.; Campbell, R. A.; Thomas, R. K.; Hook, F.; Fragneto, G.; Tiberg, F.; Nylander, T. *Soft Matter* **2008**, *4*, 2267−2277.
(15) Svensson, O.; Thuresson, K.; Arnebrant, T. *J. Colloid Interface Sci.* **2008**, *325*, 346−350.
(16) Svensson, O.; Thuresson, K.; Arnebrant, T. *Langmuir* **2008**, *24*, 2573−2579.
(17) Iler, R. K.*The chemistry of silica solubility, polymerization, colloid and surface properties, and biochemistry*; Wiley: New York, 1979; p xxiv, 866 p.
(18) Tiberg, F.; Landgren, M. *Langmuir* **1993**, *9*, 927−932.
(19) Vandoolaeghe, P.; Tiberg, F.; Nylander, T. *Langmuir* **2006**, *22*, 9169−9174.
(20) Defeijter, J. A.; Benjamins, J.; Veer, F. A. *Biopolymers* **1978**, *17*, 1759−1772.
(21) Borne, J.; Nylander, T.; Khan, A. *J. Phys. Chem. B* **2002**, *106*, 10492−10500.
(22) Vandoolaeghe, P.; Campbell, R. A.; Rennie, A. R.; Nylander, T. *J. Phys. Chem. C* **2009**, *113*, 4483−4494.
(23) Bolt, G. H. *J. Phys. Chem.* **1957**, *61*, 1166−1169.
(24) Allan, G. G.; Peyron, M. *Carbohydr. Res.* **1995**, *277*, 257−272.
(25) Guillot, M.; Richard-Plouet, M.; Vilminot, S. *J. Mater. Chem.* **2002**, *12*, 851−857.
(26) Joshi, O.; McGuire, J. *Appl. Biochem. Biotechnol.* **2009**, *152*, 235−248.
(27) Rubio, J.; Kitchener, J. A. *J. Colloid Interface Sci.* **1976**, *57*, 132−142.
(28) Dedinaite, A., Iruthayaraj, J., Gorochovceva, N., Makuska, R., Claesson, P., Grundke, K., Stamm, M., Adler, H.-J., Eds.; Interfacial properties of chitosan-PEO graft oligomers: Surface competition with unmodified chitosan oligomers. In *Progress in Colloid and Polymer Science*; Springer: Berlin, 2006; Vol. *132*, pp 124−130.
(29) Iruthayaraj, J.; Poptoshev, E.; Vareikis, A. V.; Makuska, R.; van der Wal, A.; Claesson, P. M. *Macromolecules* **2005**, *38*, 6152−6160.
(30) Stuart, M. A. C.; Tamai, H. *Langmuir* **1988**, *4*, 1184−1188.
(31) Kull, T.; Nylander, T.; Tiberg, F.; Wahlgren, N. M. *Langmuir* **1997**, *13*, 5141−5147.
(32) Neto, C.; Aloisi, G.; Baglioni, P.; Larsson, K. *J. Phys. Chem. B* **1999**, *103*, 3896−3899.
(33) Corsel, J. W.; Willems, G. M.; Kop, J. M. M.; Cuypers, P. A.; Hermens, W. T. *J. Colloid Interface Sci.* **1986**, *111*, 544−554.
(34) Tiberg, F.; Jonsson, B.; Lindman, B. *Langmuir* **1994**, *10*, 3714−3722.
(35) Reimhult, E.; Hook, F.; Kasemo, B. *J. Chem. Phys.* **2002**, *117*, 7401−7404.
(36) Reimhult, E.; Hook, F.; Kasemo, B. *Langmuir* **2003**, *19*, 1681−1691.
(37) Wacklin, H. P. *Langmuir* **2011**, *27*, 7698−7707.
(38) Weirich, K. L.; Israelachvili, J. N.; Fygenson, D. K. *Biophys. J.* **2010**, *98*, 85−92.
(39) Chang, D. P.; Jankunec, M.; Barauskas, J.; Tiberg, F.; Nylander, T. *Langmuir*, submitted for publication.